

Quantification of Constraint Loss in Three-Dimensional Non-hardening Crack-tip Fields

(Penentuan Kehilangan Kekangan dalam Medan Tiga-dimensi Hujung-retak Tiada-pengerasan)

Feizal Yusof*, Leong Karh Heng
School of Mechanical Engineering, Universiti Sains Malaysia, Nibong Tebal, 14300 Penang

ABSTRACT

Analysis of crack tip stress field is important in determining of the integrity of structures under the influence of cracks and defects. Current techniques to analyze crack tip stress fields are based on two-dimensional approach and very conservative. Efforts to develop three-dimensional crack tip stress analysis methods have been inconclusive with various drawbacks. In this paper, the structure of three-dimensional crack tip fields has been examined under non-hardening condition which will allow a detail examination of crack tip stresses in the absence of strain hardening effects. Three-dimensional crack tip analysis is based on three-dimensional bend and tension cracked models. The fields along the crack front were examined as a function of load level, J , and thickness, x_3/t . The results showed that at the crack tip ($r = 0$), a group of asymptotic fields develop which feature a constant stress sector directly ahead of the crack tip. Within this sector the fields differ hydrostatically while being similar in respect of the maximum stress deviator. From the behavior of the crack tip stresses, explicit expression of crack tip constraints are given for constraint loss in terms of maximum stresses due to out-of plane effects at and along the crack front $0 \leq x_3/t \leq 0.5$. Significantly, the results showed that constraint based fracture mechanics can be extended to fully three dimensional crack tip fields.

Keywords: Three-Dimensional Finite Element; Constraint Effects; Fracture Mechanics

ABSTRAK

Analisa medan tegasan suatu hujung retak adalah amat penting dalam memastikan integriti struktur yang dipengaruhi oleh kecacatan dan retak. Teknik yang sedia ada untuk menganalisa tegasan oleh retak didasarkan oleh kaedah dua-dimensi yang amat konservatif. Usaha-usaha untuk menghasilkan kaedah analisa bagi tegasan retak tiga-dimensi masih lagi tidak lengkap disebabkan pelbagai kelemahan. Di dalam penulisan ini, struktur tiga-dimensi medan hujung-retak telah diperiksa di bawah keadaan tiada-pengerasan yang membenarkan pemeriksaan teliti tegasan retak tanpa kesan pengerasan disebabkan oleh terikan. Analisa tiga-dimensi tegasan hujung retak dilakukan berdasarkan formulasi sempadan lapisan tiga-dimensi. Medan-medan di sepanjang retak diperiksa melalui fungsi beban, J , dan ketebalan, x_3/t . Pada hujung-retak ($r = 0$), satu kumpulan medan asimtotik terhasil yang menunjukkan sektor tegasan tetap pada hujung retak. Di dalam sektor ini, medan berbeza secara hidrostatik tetapi sama dalam penyimpangan tegasan maksima. Ungkapan yang jelas diberikan bagi kehilangan kekangan dalam tegasan maksima disebabkan oleh kesan satah terkeluar pada $\theta = 0^\circ$ dan di sepanjang retak $0 \leq x_3/t \leq 0.5$ yang menyebabkan mekanik retak berdasarkan penilaian kekangan diperpanjangkan kepada masalah hujung retak tiga dimensi. Hasil keputusan yang ketara adalah, mekanik patah berdasarkan kaedah kekangan kini boleh diunjurkan untuk menyelesaikan masalah medan hujung retak tiga-dimensi.

Kata kunci: Kaedah Unsur Terhingga Tiga-Dimensi; Kesan Kekangan; Mekanik Patah

INTRODUCTION

Constraint based fracture mechanics is based on the study of the state of elastic-plastic stresses at the crack-tip. The nature of elastic-plastic three-dimensional fields have been demonstrated independently by many different researchers and notably by (Nakamura & Parks 1990; Hom & McMeeking 1990) whereby the maximum stress occurs at the centre plane and approach the plane strain field while at the free surface, a plane stress field is recovered. The nature of the stresses were also affected by the T -stress and the

attempts to characterize the three-dimensional crack-tip fields and to estimate the constrained state have been discussed by (Nevalainen & Dodds 1995; Henry & Luxmoore 1997; Yuan & Brocks 1998; Pardo et al. 1999; Kim et al. 2003) however it has been shown that the extension of the two-dimensional plane strain (J - T/Q) technique to approximate the loss of constraint along the three-dimensional crack front is limited according to the underlying (J - T/Q) framework (O'Dowd 1995; Anderson 2005).

Other approaches to characterize the three-dimensional loss of constraint were proposed such as the J - T_z (Guo 1993),

the $J-\phi$ (Mostafavi et al. 2010), the $J-A_p$ (Yang 2013). The $J-T_z$ approach was developed based on a modified J -integral scheme to state stresses based on a T_z parameter, however the technique is dependent on finite element analysis to determine the $J-\phi$ or stresses at a given location along the crack front. In a different development, the $J-\phi$ and the $J-A_p$ were used to predict the fracture toughness of cracked specimen by semi empirical approach but do not describe the state of stresses within the deformation zone. At present a method to characterize the in-plane and the out-of-plane constraint loss is still lacking and the purpose of the current work is attempted at re-characterizing the two-parameter $J-T/Q$ approach to describe the three-dimensional crack front tip stress fields.

In the present work, the approach developed by (Betegon & Hancock 1991; O'Dowd & Shih 1991) were adopted to investigate the effect of the in-plane and the out-of-plane crack tip constraint in three-dimensional elastic-plastic crack-tip fields.

METHODOLOGY

An elastic-plastic finite element (FE) crack analysis was performed using ABAQUS v.6.12 (ABAQUS, 2012). Full field finite element SENB and CCP models were presented in this study as shown in Figure 1.

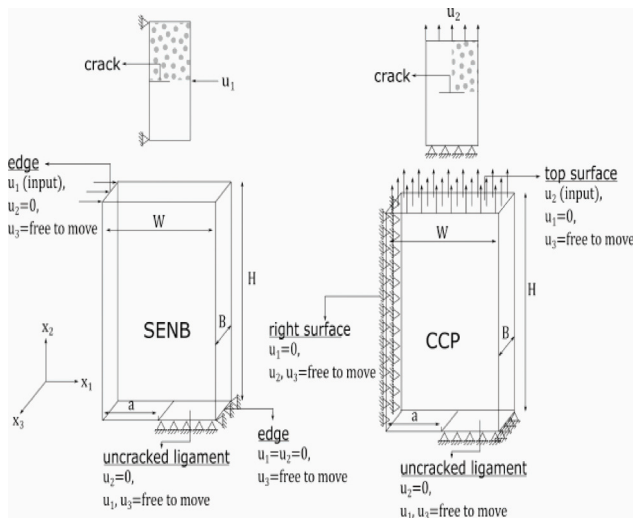


FIGURE 1. The SENB and CCP cracked models

A straight through thickness crack was modeled at the center of specimen with a crack depth to ligament length ratio, $a/W = 0.5, 0.3, 0.2$ and 0.1 . Symmetrical features allowed the mode I problem to be represented as only a quarter of the full model for the SENB and CCP models respectively. Two thickness values were employed for the models, with $B/(W-a) = 1$ and 0.05 , as representatives for a thick and a thin specimen correspondingly. The calculations were performed with a strain hardening material response, $n = \infty$ and a Poisson ratio, $\nu = 0.49$. In this study, the material responses adopted are given as shown in Equation (1):

$$\begin{aligned} \varepsilon_e &= \frac{\sigma}{E} & (\sigma < \sigma_0) \\ \frac{c_p}{\varepsilon_0} &= \left(\frac{\sigma}{\sigma_0} \right)^n & (\sigma < \sigma_0) \end{aligned} \quad (1)$$

with the Young's modulus, $E = 200$ GPa, the yield stress, $\sigma_0 = 200$ MPa and the yield strain, $\varepsilon_0 = 0.001$ while ε_p is the plastic strain and n is the strain hardening exponent.

Figure 2 shows the finite element crack tip mesh with 24 rings of 24 second order hexahedral hybrid elements with reduced integration surrounding the crack tip. The crack tip is located at a coordinate of $(0, 0)$ which consists of 49 coincident but independent nodes at any element layers along the crack front. Along the specimen thickness direction, the thickness of each element layer decreases gradually from the mid-plane ($x_3/B = 0$) to the free surface ($x_3/B = 0.5$) of the specimen as illustrated in Figure 3. The thinnest layer located at the free surface of the specimen, has a thickness of $t/B = 0.004$.

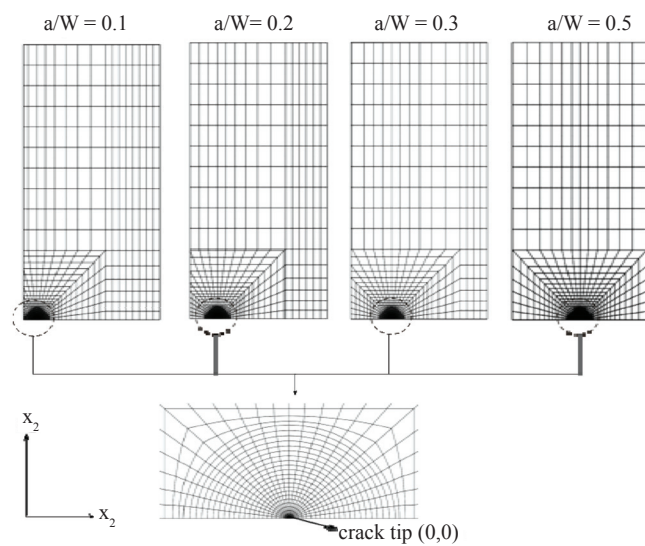


FIGURE 2. In-plane meshing pattern applied in each of the crack depth to ligament length ratio

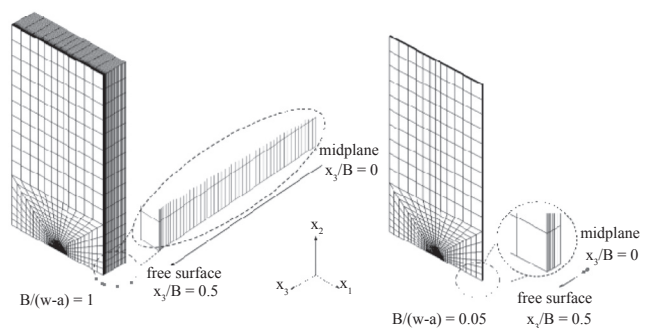


FIGURE 3. Out-of-plane FE configurations with $B/(W-a) = 1$ and 0.05

The applied load, u_p , was determined from limit load equations as described by (Miller 1988), for SENB model in Equation 2:

$$M_o = \frac{1.15W^2\sigma_o}{4} \left(1.261 \left[1 - \frac{a}{W} \right]^2 \right) \quad (2)$$

and for CCP model in Equation 3:

$$P_o = \frac{2\sigma_o(W-a)}{\sqrt{3}} \left(\frac{2}{2} \right) \quad (3)$$

The limit of load applied to the cracked specimens was governed by the J -Dominance for the associated specimens. The limit of J -Dominance is described by a non-dimensional grouping μ as shown in Equation 4:

$$\mu = (c\sigma_o)/J \quad (4)$$

where $c = (W - a)$ is the uncracked ligament and quantifies the crack tip deformation.

RESULTS AND DISCUSSIONS

First, the direct stress, σ_{22} , asymptotically around the crack tip from the mid-plane ($x_3/t = 0$) to the near the free surface ($x_3/t = 0.49$) is shown in Figure 4. The stresses in Figure 4 have been compared to a two-dimensional plane strain fully constrained stress field which is shown as a dashed line. It is shown that the direct stress σ_{22} for a three-dimensional crack tip fields approached the Prandtl field at the mid-plane and approach the plane stress field at the free surface. The nature at which the constraint is lost is characterized by a hydrostatically different stress across the thickness within the sector $\theta \leq 45^\circ$ which showed that the hoop stress drops consistently with distance from the mid-plane towards the free surface. Similar behavior is demonstrated for SENB and CCP models. For the CCP models, the maximum stress lose the in-plane constraint readily and the out-of-plane constraint drops consistent across the thickness.

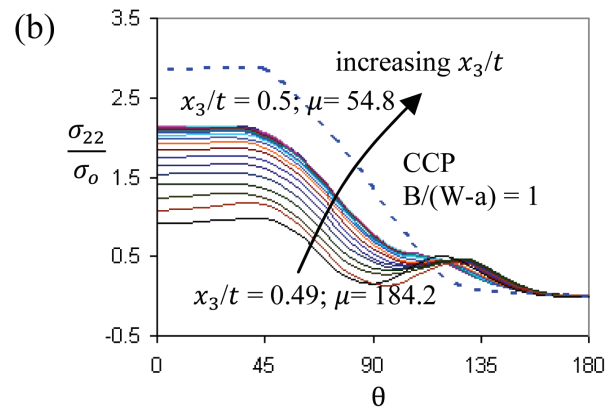
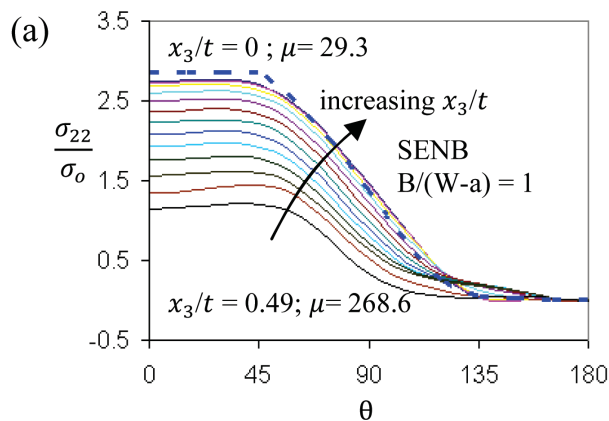


FIGURE 4. The asymptotic direct stress, σ_{22}/σ_o around a three-dimensional SENB and CCP models

Figure 5 shows the state of the deviatoric stress around the crack tip with the sector ahead of the crack and ahead of the crack tip along a three-dimensional crack front. It is shown that the deviatoric stress is similar in the forward sector of the crack front tip.

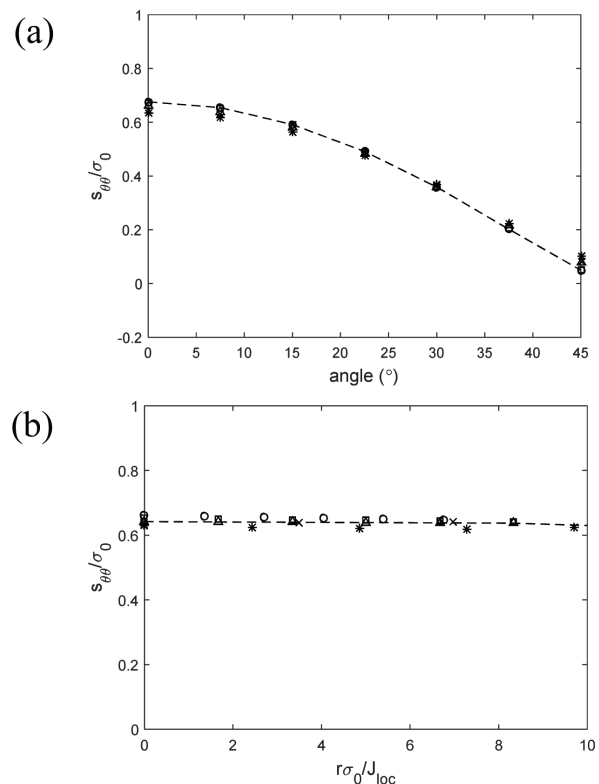


FIGURE 5. The hoop stress deviator at $0^\circ < \theta < 45^\circ$ and ahead of a three-dimensional crack front along $0 < x_3/t < 0.5$ for SENB and CCP models

Both state of stresses satisfy the basic two conditions set for the $J-T/Q$ approach however the third conditions which is the direct stresses ahead of the crack have to be distance independent cannot be satisfied for three-dimensional crack tip fields. (Yusof 2006) demonstrated that direct stresses along a three-dimensional crack front tip was independent of x_2/t at fixed distance ahead of the crack front tip. Figure 6 shows the state of the hoop stress at a given distance ahead of the crack front and along the crack front which can be related uniquely as a function of J and distance along the crack front.

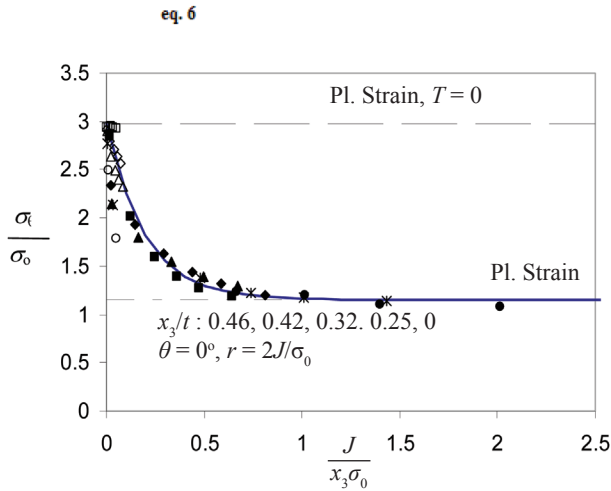


FIGURE 6. The hoop stress for SENB ($B/W - a = 1$ and 0.1) at $r = 2J/\sigma_0$ along the crack front

The curve (Figure 6) shows that stress drop from a fully constrained level associated with a plane strain, $T = 0$ field. The stress then drops according to an exponential curve and approach a plane stress field at the free surface.

Figures 4 to 6 demonstrate that a three-dimensional crack tip field can fulfill the condition for a two-parameter fracture mechanics framework because the crack tip stress field is hydrostatically different but stress is deviatorically similar ahead of the crack tip front. More importantly the stresses were shown to be independent of distance when stresses were plotted at a distance ahead of the crack but varied with the distance along the crack front tip.

Constraint Estimation Scheme for $\sigma_{\theta\theta}$ at $\theta = 0^\circ$

The state of finite stresses for elastic-perfectly plastic non-hardening materials can be utilized to predict stresses along a three-dimensional crack front tip. Figure 7 show the distribution of $\sigma_{\theta\theta}$ at angle, $\theta = 0^\circ$ along the crack front of the models with thickness, $B/(W - a) = 1$ from the midplane ($x_3/B = 0$) to the free surface ($x_3/B = 0.5$). From the mid-plane, the hoop stresses in the SENB and CCP models gradually reduces towards the free surface due to the out-of-plane constraint loss. In the region $x_3/B \geq 0.35$, $\sigma_{\theta\theta}$ in the thick SENB and CCP models approach a unique constraint loss toward the free surface.

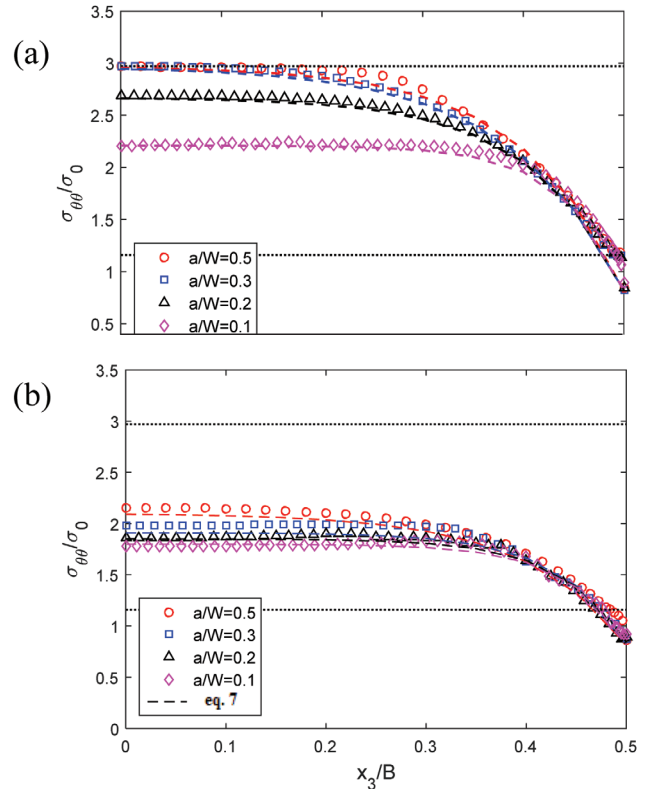


FIGURE 7. Distribution of $\sigma_{\theta\theta}$ at $\theta = 0^\circ$ and $r = 0$ along the crack of a) SENB, b) CCP models ($B/(W - a) = 1$) with $a/W = 0.5, 0.3, 0.2$ and 0.1

To approximate $\sigma_{\theta\theta}$ along the crack front at $\theta = 0^\circ$ of the thick SENB and CCP models as shown in Figure 7, an analytical expression is developed based on the relationship between the constraint loss and T -stress at the mid-plane. The constraint loss denoted as Q_c is firstly defined as the difference of from the midplane of models ($x_3/B = 0$) and the Prandtl field value at $\theta = 0^\circ$ in Equation 5:

$$Q_c = \frac{\sigma_{\theta\theta(\text{prandtl})}}{\sigma_0} - \frac{\sigma_{\theta\theta(\text{FE}, x_3/B=0)}}{\sigma_0} \quad (r = 0, \theta = 0^\circ) \quad (5)$$

Then, the values of Q_c of the thick models are plotted with respect to the normalized T -stress, T/σ_{app} in Figure 8. The correlation between Q_c and T/σ_{app} in the thick SENB models can be described by the expressions as follows:

$$Q_c = 0 \quad \left(\frac{T}{\sigma_{app}} \geq 0 \right)$$

$$Q_c = 8 \left(\frac{T}{\sigma_{app}} \right)^2 - 0.19 \left(\frac{T}{\sigma_{app}} \right) + 0.013; \quad \left(\frac{T}{\sigma_{app}} < 0 \right) \quad (6)$$

Meanwhile, the polynomial expression for the Q_c of the thick CCP models is given as:

$$Q_c = 0.97 \left(\frac{T}{\sigma_{app}} \right)^2 - 0.043 \left(\frac{T}{\sigma_{app}} \right) + 0.0058; \quad \left(\frac{T}{\sigma_{app}} < 0 \right) \quad (7)$$

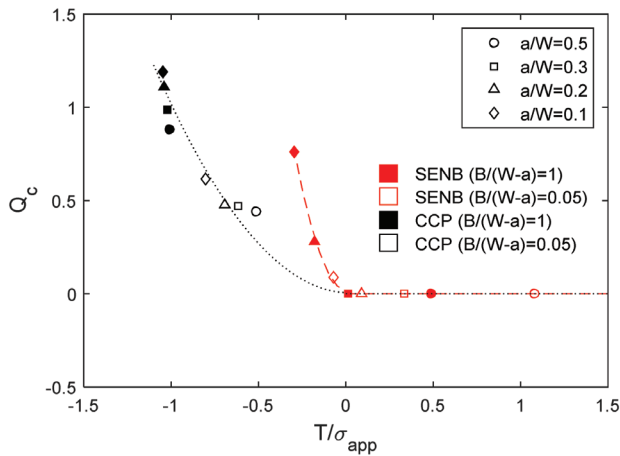


FIGURE 8. Fitting curve for Q_c against T/σ_{app} at the midplane of the SENB and the CCP models ($B/(W - a) = 1$)

Using Q_c approximated from equations 6 and 7, the distribution of $\sigma_{\theta\theta}$ along the crack front of the thick SENB and CCP models can be estimated via the following expression in Equation 8:

$$\frac{\sigma_{\theta\theta}}{\sigma_0} = (a + 2b) - \left[(a - b) \exp \left(-c_i \left(0.5 - \frac{x_3}{B} \right) + b \right) \right]; \quad (8)$$

$$\left(0 \leq \frac{x_3}{B} \leq 0.5 \right); \quad a = 2.97 - Q_c \quad b = 0.84$$

where c_i is a constant which depends on the crack configuration. The values of c_i in equation 8 are tabulated in Table 1. The fitting curves plotted for the thick SENB and CCP models using equation 8 are shown as dashed lines in Figure 8.

The distribution of $\sigma_{\theta\theta}$ along the crack front of the thin models, ($B/(W - a) = 0.05$) is shown in Figure 10. The distribution of $\sigma_{\theta\theta}$ for each a/W ratio of the thin models is relatively close to each other. The deviation of $\sigma_{\theta\theta}$ from the fully constraint Prandtl value in the thin SENB models with $a/W = 0.1$ and 0.2 are smaller than that in the thick SENB models because of the smaller in-plane constraint loss since they feature higher magnitude of T -stresses as shown in Figure 9a. Such trend is also found in the thin CCP models. The thin CCP models possess less compressive T -stresses (see Figure 9b), resulting in higher $\sigma_{\theta\theta}$ along the crack front than that in the thick CCP models.

TABLE 1. Values of c_i for each crack configuration in the models with $B/(W - a) = 1$

a/W	Value of	
	SENB	CCP
0.5	9	10
0.3	10	15
0.2	11	16
0.1	17	17

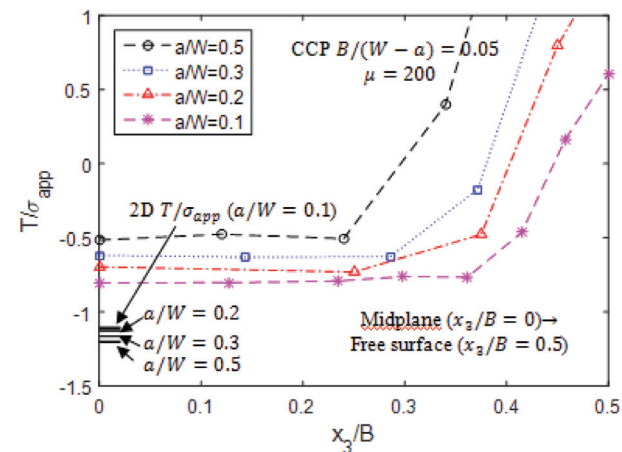
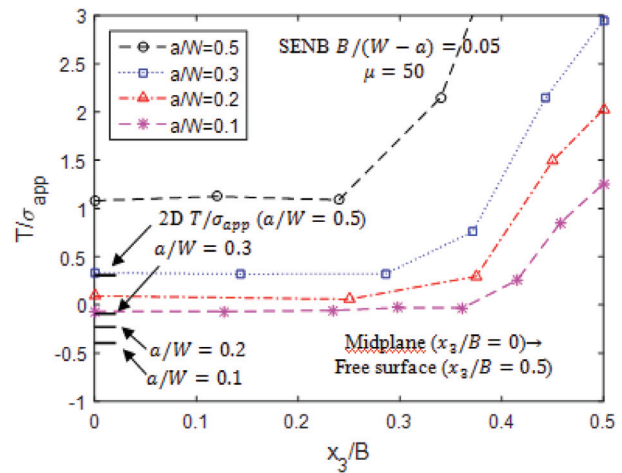


FIGURE 9. Thickness distribution of -stress in the SENB and CCP models

The distribution of $\sigma_{\theta\theta}$ along the crack front of the thin SENB and CCP models can be estimated by the following analytical formula:

$$\frac{\sigma_{\theta\theta}}{\sigma_0} = (2.97 - Q_c) \exp \left[- \left(\frac{\left(\frac{x_3}{B} - d \right)^2}{0.52(\quad)} \right) \right]; \quad (9)$$

$$\left(0 \leq \frac{x_3}{B} \leq 0.5 \right)$$

where d is a constant which has a value of 0.003 for the thin SENB models and 0.055 for the thin CCP models. The fitting curves plotted for the thin SENB and CCP models using equation 9 are shown in Figure 10.

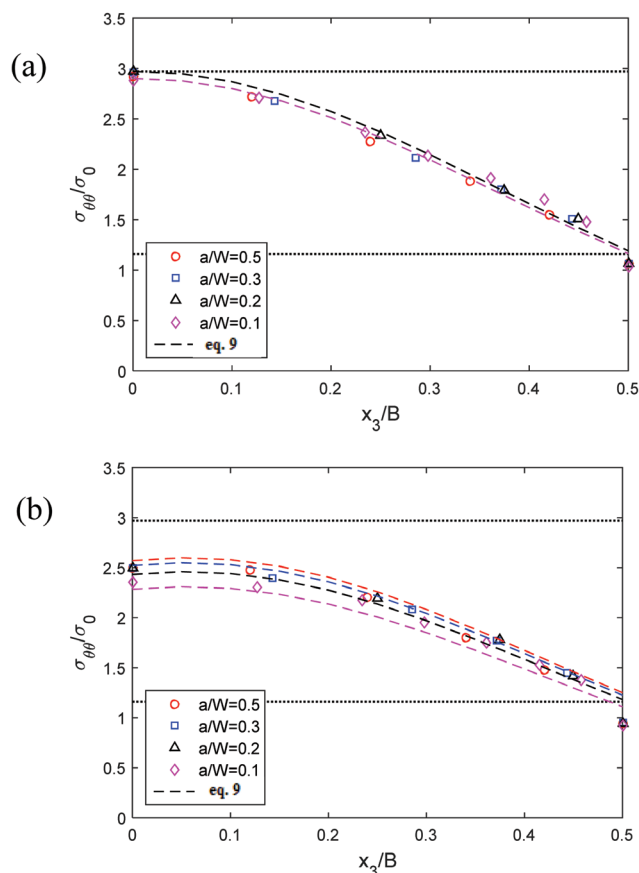


FIGURE 10. Distribution of $\sigma_{\theta\theta}$ at $\theta = 0^\circ$ and $r = 0$ along the crack front of a) SENB, b) CCP models ($B/(W-a) = 0.05$) with $a/W = 0.5, 0.3, 0.2$ and 0.1

CONCLUSIONS

Crack tip constraint is important because it affects fracture toughness and hence defect tolerance. The nature of three-dimensional crack tip fields has been shown to be formed by a group of fields which differ hydrostatically but is similar in respect of the maximum stress deviator. In-plane constraint loss effects are distance (r) independent, but out-of-plane constraint loss arises from decay in the mean stress, σ_m , with distance from the crack tip. Despite the decay in the mean stress, σ_m , and the opening stress, σ_{22} , the maximum stress deviator, s_{22} , remains independent of distance, r , and position along the crack front, x_3 . Explicit expressions are given enabling constraint loss to be determined due to out-of-plane constraint loss. As this allows for the in-plane effects, it is applicable for all three dimensional configurations and establishes a basis for extending constraint based fracture mechanics into three dimensional fields.

ACKNOWLEDGEMENTS

The present study is carried out through a Ministry of Higher Education (MOHE) grant FRGS 2016/F1123). The ABAQUS finite element code was made available under an academic license from Dassault Systemes K. K.

REFERENCES

- Abaqus 2012. Abaqus ver 6.12 User's Manual. Kaigan Minato-ku Tokyo, Japan: Dassault Systemes, K. K.
- Anderson, T.L. 2005. *Fracture Mechanics: Fundamentals and Applications*. Boca Raton. CRC Press.
- Betegon, C. & Hancock, J.W. 1991. Two-parameter characterization of elastic-plastic crack-tip fields. *Journal of Applied Mechanics-Transactions of the Asme* 58(1): 104-110.
- Guo, W.L. 1993. Elastoplastic 3-dimensional crack border field.1. singular structure of the field. *Engineering Fracture Mechanics* 46: 93-104.
- Henry, B.S. & Luxmoore, A.R. 1997. The stress triaxiality constraint and the Q-value as a ductile parameter. *Engineering Fracture Mechanics* 57(4): 375-390.
- Hom, C.L. & Mcmeeking, R.M. 1990. Large crack tip opening in thin elastic-plastic sheets. *International Journal of Fracture* 45(2): 103-122.
- Kim, Y., Chao, Y.J. & Zhu, X.K. 2003. Effect of specimen size and crack depth on 3D crack-front constraint for SENB specimens. *International Journal of Solids and Structures* 40(23): 6267-6284.
- Miller, A.G. 1988. Review of limit load for structures containing defects. *International Journal of Pressure Vessels and Piping* 32(1-4): 197-327.
- Mostafavi, M., Smith, D.J. & Pavier, M.J. 2010. Reduction of measured toughness due to out-of-plane constraint in ductile fracture of aluminium alloy specimens. *Fatigue & Fracture of Engineering Materials & Structures* 33(11): 724-739.
- Nakamura, T. & Parks, D.M. 1990. Three-dimensional crack front fields in a thin ductile plate. *Journal of the Mechanics and Physics of Solids* 38(6): 787-812.
- Nevalainen, M. & Dodds, R.H. 1995. Numerical investigation of 3-D constraint effects on brittle fracture in SE(B) and C(T) specimens. *International Journal of Fracture* 74(2): 131-161.
- O'dowd, N.P. 1995. Application of two parameter approaches in elastic plastic fracture mechanics. *Engineering Fracture Mechanics* 52(3): 445-465.
- O'dowd, N.P. & Shih, C.F. 1991. Family of crack-tip fields characterized by a triaxiality parameter, Part I - Structure of fields. *Journal of the Mechanics and Physics of Solids* 39(8): 989-1015.
- Pardoen, T., Marchal, Y. & Delannay, F. 1999. Thickness dependence of cracking resistance in thin aluminium plates. *Journal of the Mechanics and Physics of Solids* 47(10): 2093-2123.
- Yang, J., Wang, G., Xuan, F. & Tu, S. 2013. Unified characterisation of in-plane and out-of-plane constraint based on crack-tip equivalent plastic strain. *Fatigue & Fracture of Engineering Materials & Structures* 36(6): 504-514.
- Yuan, H. & Brocks, W. 1998. Quantification of constraint effects in elastic-plastic crack front fields. *Journal of the Mechanics and Physics of Solids* 46(2): 219-241.

Yusof, F. 2006. *Three-dimensional constraint based fracture mechanics*. Ph.D, University of Glasgow.

*Feizal Yusof, Leong Karh Heng
School of Mechanical Engineering,
Universiti Sains Malaysia,
Nibong Tebal 14300, Penang.

*Corresponding author; email: mefeizal@usm.my

Received date: 16th July 2018

Accepted date: 6th August 2018

Online First date: 1st October 2018

Published date: 30th November 2018